Manipulating charge ordering in Fe_3O_4 by field cooling

T. P. Ma,[1,3] Y. Yang,[1] Z. Ding,[1] Z. H. Chen,[1,5] H. B. Zhao,[2,*] P. Werner,[3] Stuart S. P. Parkin,[3,4] and Y. Z. Wu[1,5,†]

[1]*Department of Physics, State Key Laboratory of Surface Physics, Fudan University, Shanghai 200433, China*

[2]*Key Laboratory of Micro and Nano Photonic Structures (Ministry of Education), and Shanghai Ultra-precision Optical Manufacturing Engineering Research Center, Department of Optical Science and Engineering, Fudan University, Shanghai 200433, China*

[3]*Max Planck Institute for Microstructure Physics, Halle (Saale) D-06120, Germany*

[4]*IBM Almaden Research Center, 650 Harry Road, San Jose, California 95120, USA*

[5]*Collaborative Innovation Center of Advanced Microstructures, Nanjing 210093, China*

(Received 4 November 2015; revised manuscript received 29 November 2016; published 6 January 2017)

The conductivity of Fe_3O_4 drops two orders of magnitude below the Verwey temperature T_v, known as the Verwey transition, due to the formation of charge ordering (CO). Here, we report the discovery of a large birefringence effect correlated with the CO in Fe_3O_4 controlled by ultrafast-laser-assisted magnetic field cooling. The polarization rotation (PR) of the light reflected from a single crystalline Fe_3O_4 film below T_v shows a twofold symmetry as the cooling field (CF) rotates through 360° within the film plane. The maximum PR occurs for the CF parallel to the cubic ⟨110⟩ axes, and its amplitude depends on the sample orientation. These results are well interpreted by taking into account two CO patterns with orthogonal CO orientations, with their fractional areas determined by the ratio of the field components along the [110] and [1$\bar{1}$0] axes. Our results indicate that application of the CF along ⟨110⟩ axes may result in the single orientation CO state, which is highly desirable for unraveling the subtle CO structure to better understand the driving mechanism of the Verwey transition. In addition, ultrafast pump-probe measurements reveal a diminishment of the twofold PR at 0.8 ps due to fast melting of the CO state by the ultrafast laser pulse.

DOI: 10.1103/PhysRevB.95.014103

I. INTRODUCTION

Charge ordering (CO) [1] has a profound impact on the transport properties of strongly correlated metal oxide systems. The CO formation drives the metal-insulator transition in magnetite (Fe_3O_4) [2–4] and colossal magnetoresistance manganite materials [5–7]. Furthermore, CO also plays a crucial role in superconducting materials [8,9] and quasi-two-dimensional systems [10,11]. Among various metal oxide systems, magnetite has the oldest history but is still under intensive study [12–15]. In 1939, Verwey found that magnetite's conductivity rapidly drops two orders of magnitude below $T_v \sim 125$ K [16,17], and currently it is widely believed that the conductivity drop is primarily due to the ordered pattern of Fe^{2+} and Fe^{3+} ions in the octahedral sites [13,18,19]. Accompanied by the formation of CO, magnetite also experiences a lattice distortion from the cubic to the monoclinic structure [20,21], with the monoclinic *a* and *b* axes along the ⟨110⟩ directions and the *c* axis along the ⟨100⟩ directions. Because the monoclinic *c* axis can be along any of the cubic ⟨100⟩ directions, multidomains may form below T_v in bulk Fe_3O_4 [22,23]. Below T_v, the separated Fe^{2+} (Fe^{3+}) chains are oriented along the cubic [110] or [1$\bar{1}$0] axis in the case of the monoclinic *c* axis [001] normal to the film plane, yielding two major orthogonal CO patterns. To better understand the driving mechanism of the Verwey transition, it is strongly desired to control the orientations of the *c* axis and the CO. A quasisingle domain of monoclinic structure can be achieved by applying a magnetic field along one of the ⟨100⟩ directions when cooling bulk Fe_3O_4 below T_v [24,25]. The monoclinic *c* axis is then parallel to the cooling field (CF) direction. In spite of the long history of CF control of the *c* axis, control of the CO orientation has yet to be demonstrated.

In this paper, we present evidence that field cooling induced by an ultrafast laser can control CO orientations in a single-crystalline Fe_3O_4 film. When below T_v, the polarized light reflected from the Fe_3O_4 film experiences a pronounced polarization rotation (PR) with a twofold symmetry when rotating the CF 360° within the film plane. Such a twofold PR signal induced by field cooling exists only at temperatures below T_v. This effect can be interpreted by taking into account the fractional areas of the two CO patterns with orthogonal CO orientations, which are determined by the ratio of the field/magnetization components along the [110] and [1$\bar{1}$0] directions. Our results therefore suggest that application of a CF along the in-plane ⟨110⟩ axes of a single-crystalline Fe_3O_4 film may yield the CO pattern with its CO orientation only along the CF. In addition, the ultrafast pump-probe measurements identified that the time scale of CO melting by the ultrafast laser pulse is less than 0.8 ps.

II. EXPERIMENT

Single crystalline Fe_3O_4 films were deposited on MgO (001) substrates by evaporating Fe atoms with an oxygen pressure of 5×10^{-6} Torr at 250 °C in an ultrahigh vacuum chamber [26,27]. The film thickness was determined by the growth rate measured by a calibrated quartz thickness monitor. The sharp stripes of the reflection high-energy electron diffraction (RHEED) patterns in Figs. 1(a) and 1(b) prove the high-quality epitaxial growth of Fe_3O_4 films. The morphology and crystal structure of our film were further characterized by transmission electron microscopy (TEM), as shown in Figs. 1(d) and 1(e). We used a JEOL JEM-4010

*hbzhao@fudan.edu.cn

†wuyizheng@fudan.edu.cn

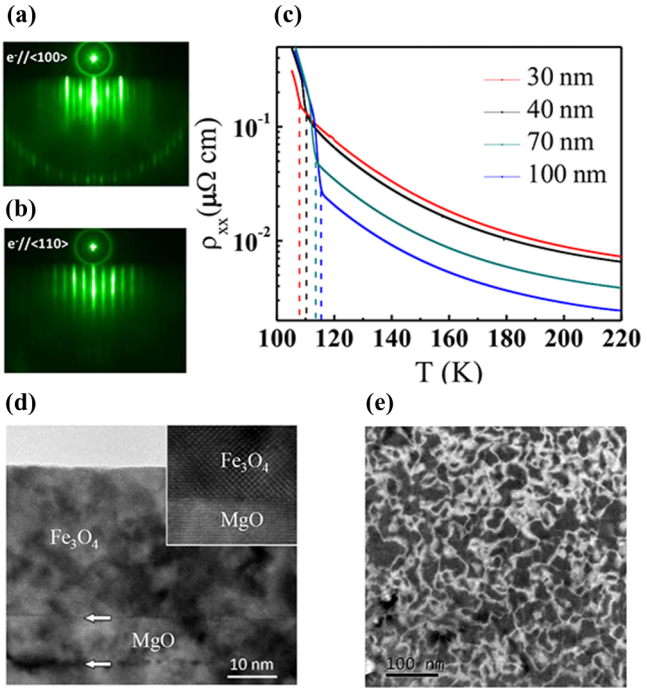

FIG. 1. (a), (b) The RHEED patterns of 30-nm-thick Fe_3O_4 film on MgO(001). (c) Temperature dependence of the resistivity of Fe_3O_4 films with different thicknesses. (d) Cross-section high-resolution TEM image of a 30-nm-thick Fe_3O_4 film on MgO(001). Interfaces between the 30 nm Fe_3O_4 layer, the 10 nm MgO seed layer, and the MgO substrate are indicated by arrows. The inset shows the good epitaxial growth of the film with sharp interface and (e) dark-field plane-view TEM image of the same sample showing the antiphase boundaries.

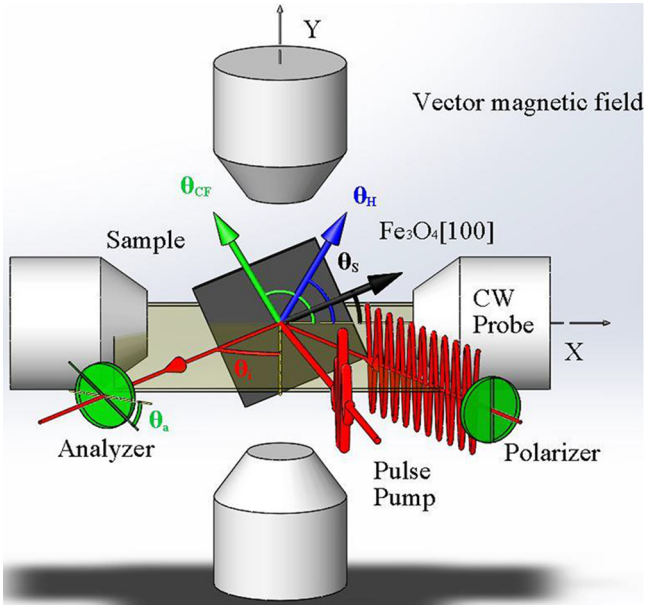

FIG. 2. Schematic drawing of the experiment setup, where θ_i represents the incident angle of the probe beam. θ_H, θ_{CF}, and θ_s denote the angle of the external field, the cooling field, and the [100] axis of the sample with respect to the horizontal x axis, respectively.

working at 400 kV acceleration voltages. Cross-section as well as plane-view samples have been prepared by conventional technology. The clear atomic pattern in the cross-section TEM image indicates a good epitaxial growth of the Fe_3O_4 film on the MgO substrate. In Fig. 1(c), temperature-dependent transport measurement reveals a sharp resistivity change near $T_v \sim 107$ K for the 30-nm-thick film, confirming the Verwey transition. We observed that the T_v becomes higher as the film thickness increases [28,29]. The T_v of the Fe_3O_4 film in this paper is similar to that of the 40-nm-thick film reported in Ref. [30]. The lower transition temperature in the thin film than in bulk Fe_3O_4 is usually attributed to the different thermal expansion between the film and the substrate [30] and the presence of antiphase boundaries (APBs) [28]. The dark-field plane-view TEM image in Fig. 1(e) confirms the existence of APBs in our sample, and the average APB domain size was analyzed as ∼35 nm, which is similar to that reported in Ref. [31] with the same film thickness. Usually, the APB domain size increases with the film thickness [31].

For static PR measurements, we directed an s-polarized continuous wave (CW) laser ($\lambda = 670$ nm) on the sample with an incident angle of 45° and measured the reflected light passing through an analyzer with its polarization within the horizontal incident plane. Figure 2 shows the schematic illustration of the setup to measure the PR induced by CO as well as the magneto-optic Kerr effect (MOKE) [32]. When the offset angle θ_a of the analyzer was set at a few degrees away from the extinction angle of the reflection beam, the change of the light intensity in the detector was proportional to the PR angle δ. By adding a quarter-wave plate between the sample and the analyzer, the ellipticity can be measured [32]. The sample was placed in a dewar that could control the sample temperature from 80 K to 300 K. A vector magnetic field was applied along arbitrary directions in the sample plane to serve as the CF, or external field (H) [33]. We define the sample orientation θ_s, CF direction θ_{CF}, and H direction θ_H as the angle of the [100] axis, CF, and H with respect to the horizontal x axis, respectively, as shown in Fig. 2. To speed up the static PR measurements with various θ_{CF}, we implemented laser-assisted field cooling using femtosecond (fs) laser pulses. In this process, we kept the sample at the measured temperature below T_v with a CF of 1000 Oe applied along the desired direction and directed a few fs laser pulses (150 fs, 800 nm, 1 kHz, and ∼2 mJ cm^{-2}) on the sample to instantly heat it to above T_v. The film was then cooled down to the measured temperature after heat diffusion within 1 ms. Each laser pulse in the pulse train actually reproduces the same field cooling process.

For ultrafast pump-probe measurements, the pump pulses (∼2 mJ cm^{-2}) with a 1 kHz repetition rate were nearly perpendicularly incident on the sample. The probe beam (∼0.1 mJ cm^{-2}) with spot diameter of 0.5 mm was spatially overlapped with the pump beam on the sample. We used s-polarized probe light at an incident angle of 45° to probe the PR angle δ, with the same beam path used in the static PR measurements.

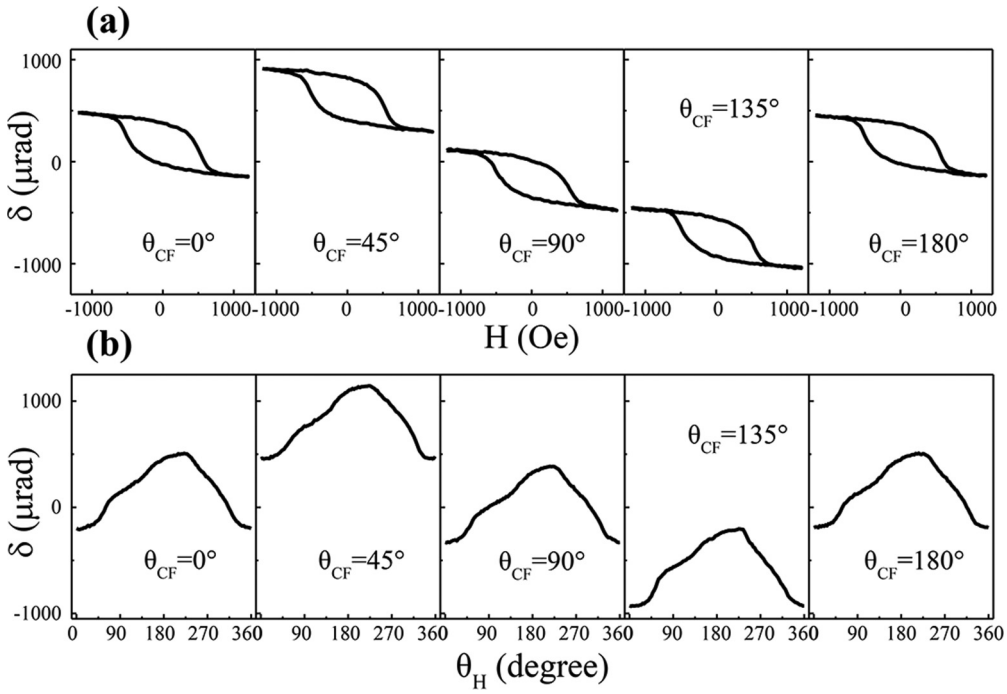

FIG. 3. The PR angle δ for (a) H_E sweeping along the [100] direction ($\theta_H = 0^\circ$), and (b) $H_E = 1000$ Oe rotated 360° at $T = 80$ K, $\theta_s = 0^\circ$, and varying θ_{CF}.

III. RESULTS

Figure 3(a) shows the PR angle δ of a 30-nm-thick Fe_3O_4 film measured at $T = 80$ K under the conditions of $\theta_s = 0^\circ$, H sweeping between ± 1200 Oe at $\theta_H = 0^\circ$, and various θ_{CF}. A clear feature in Fig. 3(a) is the hysteresis loop, which arises from the MOKE and corresponds to the magnetization reversal process. All these loops show nearly identical shapes and magnitudes, indicating a similar magnetization reversal process. However, the center of the hysteresis loops shifts vertically with respect to each other. This shift is even larger than the Kerr angle. By plotting the center of hysteresis loop, denoted δ_c, as a function of θ_{CF} from 0° to 360° [Fig. 4(a)], we can clearly see a twofold symmetry, with maxima at $\theta_{CF} = 45^\circ$ and 225°, i.e., CF along the ⟨110⟩ axes. This twofold δ_c can be well fitted by a sinusoidal function $A_2 \sin(\theta_{CF})$, which will be further discussed below. Here, A_2 denotes the amplitude of the twofold δ_c.

After each field cooling process with different θ_{CF}, we also measured the PR signal as a function of θ_H with $H = 1$ kOe and $\theta_s = 0^\circ$. It is well known that the Kerr signal changes with the magnetization orientation driven by the external field, and the shape of the $\delta(\theta_H)$ curve is determined by the magnetic anisotropy of the film. As shown in Fig. 3(b), except for shifting vertically with respect to each other, the measured $\delta(\theta_H)$ curves with different θ_{CF} show nearly identical shape, indicating that the different CF direction results in the same in-plane magnetic anisotropy.

To understand the origin of the twofold δ_c, we further performed the above PR measurements at various sample temperatures. Figure 4(a) shows δ_c as a function of θ_{CF} for various temperatures [34], where we can also see a twofold symmetry at 104 K, but its amplitude is smaller than that at 80 K. In contrast, no twofold δ_c is observed at 109 K. Figure 4(b) shows that the amplitude of the twofold δ_c gradually decreases with increasing temperature and sharply drops to zero near 107 K. The sharp transition temperature agrees well with the T_v observed from the conductivity measurements shown in Fig. 1(c), so it is reasonable to

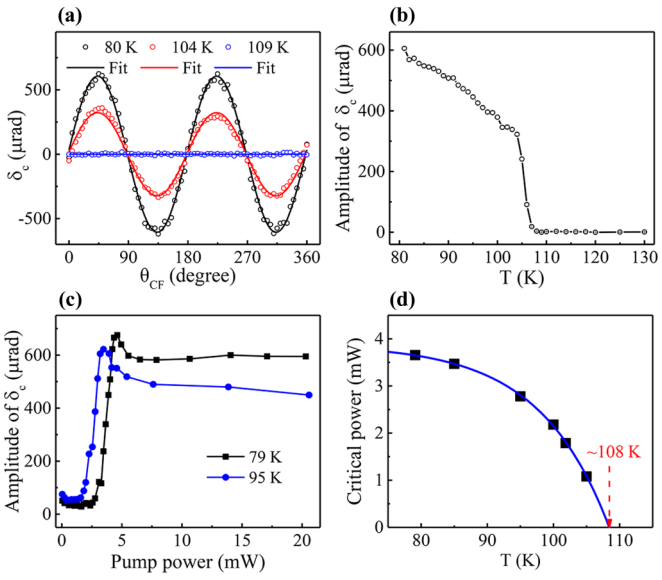

FIG. 4. (a) The twofold δ_c vs θ_{CF} at various temperatures with $\theta_s = 0^\circ$, and the solid curves are fits with the function $A_2 \sin(2\theta_{CF})$. (b) Temperature dependence of the amplitude of the twofold δ_c. (c) Amplitude of the twofold PR signal at different temperatures as a function of the pump laser power and (d) temperature dependence of the critical laser power to induce the twofold PR signal. The sample orientation was set at $\theta_s = 0^\circ$. The solid line in (d) is a visual guide.

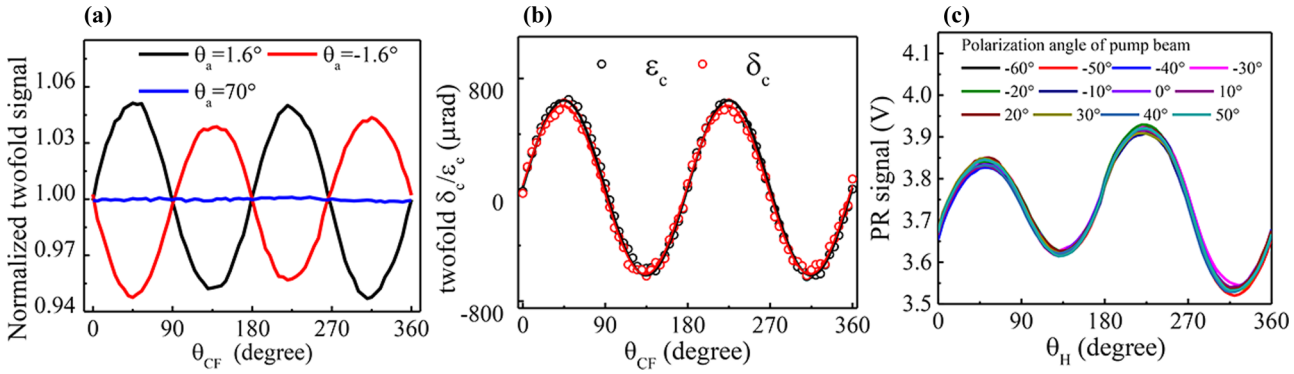

FIG. 5. (a) The twofold signal as a function of the CF direction θ_{CF} at $\theta_s = 0^\circ$ and $T = 80$ K for different θ_a. (b) Comparison of the polarization rotation angle δ_c and ellipticity ε_c with the twofold symmetry at $\theta_s = 0^\circ$. (c) The PR signal as a function of the field orientation for different pump polarizations at $T = 80$ K. The measurements in (c) were performed with the pump pulse always on at $\theta_s = 0^\circ$.

conclude that the emergence of the twofold δ_c should be caused by the electronic, structural, or magnetic order transition across T_v. It is also reasonable for the twofold δ_c to decrease with the temperature, as the electron localization in the separated Fe^{2+}/Fe^{3+} chains increases with decreasing temperature [35].

To further confirm the correlation between the observed twofold PR and the field cooling through T_v, we measured the twofold signal to obtain its amplitude as a function of the intensity of the pump light at different temperatures, as shown in Fig. 4(c). It is clear that the pump light has a threshold intensity to induce the twofold PR signal, whose amplitude becomes nearly constant with stronger pump light. The threshold power of the pump laser is lower if measured at higher temperature. We define the critic power as the pump power under which the twofold amplitude is half of the maximum value and plot the temperature-dependent critic power in Fig. 4(d). The critic power obviously decreases with the measurement temperature and extrapolates to zero at the temperature of ~108 K, which is close to T_v. This result further confirms that the emergence of the twofold PR signals is related to the Verwey transition. The twofold PR signal can exist only with the pump light strong enough to heat the sample above T_v, so it requires a power threshold of the pump light. The threshold intensity decreases with the temperature and approaches zero at $\sim T_v$.

It should be emphasized that the measured twofold signals shown in Fig. 3 are really due to the polarization change of the reflected light. The twofold signal is reversed when θ_a changes from 1.6° to −1.6°, as shown in Fig. 5(a). When θ_a is set close to 90°, the measured signal should be insensitive to the small change of PR angle and is only proportional to the total reflected light intensity. So the measured signal with $\theta_a = 70^\circ$ being independent of θ_{CF} [see Fig. 5(a)] proves that the total reflected light intensity is not influenced by the field cooling. We also measured the polarization ellipticity by inserting a quarter-wave plate in the reflected beam path and compared it with the PR angle [Fig. 5(b)]. The measured ellipticity shows a similar behavior of a twofold signal as a function of θ_{CF}.

Moreover, we found that the observed twofold PR signal does not change with the linear polarization orientation of the pump pulse, as shown in Fig. 5(c), which can confirm the heating effect of the pump light. In this measurement, the field angle θ_H during the measurement was set equal to θ_{CF}, different from the experiments shown in Figs. 3 and 4, in which θ_H was always fixed as 0°. Here the magnetization rotates with θ_{CF}, thus the total signal should contain the twofold signal of the PR due to the field cooling and a onefold signal due to the magnetization rotation. The results in Fig. 5(c) show that both the twofold signal and the onefold signal are independent of the polarization orientation of the pump pulse.

IV. DISCUSSION

A. Origin of the PR signal with twofold symmetry

As shown Fig. 3, the measured magnetic Kerr signal doesn't change with the different CF orientation, which strongly suggests that the obtained PR signal below T_v is related to the electronic structure or the atomic structure. It is well known that below T_v, the CO exists. The detailed structure of the CO is still under debate [18,19,36,37], and both the monoclinic $P2/c$ structure and the Cc structure were proposed in the literature. In both structures, the separated Fe^{2+} (Fe^{3+}) chains are oriented along the cubic [110] or [1$\bar{1}$0] axis in the case of the monoclinic c axis normal to the film plane. Figure 6 shows the typical CO patterns of Fe_3O_4 with the separated Fe^{2+}(Fe^{3+}) chains along the [110] and [1$\bar{1}$0] axes in a monoclinic $P2/c$ structure or in a Cc structure. In both cases, the CO could orient along either the [110] axis or the [1$\bar{1}$0] axis within the same atomic structure, yielding two major orthogonal CO patterns. In each CO pattern, the separate Fe^{2+} (Fe^{3+}) chains are locked along the a axis [37–39], thus the a axis in each CO pattern follows the CO orientation.

In a CO pattern with a single CO orientation, the CO will break the symmetry between the [110] and [1$\bar{1}$0] axes and thus could induce a birefringence with the optic axis along the [110] or [1$\bar{1}$0] axes. Such a birefringence effect will induce an additional PR signal for the light reflected from the area with the single orientation CO pattern. For the incident light with s polarization, it may split into two components with the electric field oscillating parallel and perpendicular to the CO orientation, which experience the different indices of refraction $\tilde{n}_1$ and $\tilde{n}_2$. The PR angle and ellipticity of the light propagating

within the film should be described as

$$\delta + i\varepsilon = \frac{E\cos\left(\frac{\pi}{4}-\theta_s\right)\sin\left(\frac{\pi}{4}-\theta_s\right)e^{i\tilde{n}_1 d} - E\sin\left(\frac{\pi}{4}-\theta_s\right)\cos\left(\frac{\pi}{4}-\theta_s\right)e^{i\tilde{n}_2 d}}{E\cos^2\left(\frac{\pi}{4}-\theta_s\right)e^{i\tilde{n}_1 d} + E\sin^2\left(\frac{\pi}{4}-\theta_s\right)e^{i\tilde{n}_2 d}} \approx (\delta_0 + i\varepsilon_0)\cos 2\theta_s, \quad (1)$$

where $\delta_0 + i\varepsilon_0 = \frac{e^{i\tilde{n}_1 d} - e^{i\tilde{n}_2 d}}{e^{i\tilde{n}_1 d} + e^{i\tilde{n}_2 d}}$, E is the electric field of the incident light, and d is the film thickness. Thus, the PR angle and ellipticity are maximal for the ⟨100⟩ axes along the light polarization, i.e., $\theta_s = 0^\circ$ or 90°, and become zero for the ⟨110⟩ axes along light polarization, i.e., $\theta_s = 45^\circ$ or 135°.

In general, for the Fe_3O_4 (001) film with its c axis normal to the plane, the [110] and [1$\bar{1}$0] axis are equivalent because the two CO patterns with the CO orientation along the [110] or [1$\bar{1}$0] axis should be randomly distributed in the film. The birefringence effects from the [110] and [1$\bar{1}$0] CO patterns should cancel each other, thus no PR signal can be expected. Here, we propose that the field cooling could break the balance of the [110] and [1$\bar{1}$0] CO patterns in the Fe_3O_4 film, and the fractional areas of the two orthogonal CO patterns can be controlled by the CF directions with respect to the ⟨110⟩ crystalline directions. After field cooling with a strong enough CF, the fractional areas of the two orthogonal CO states can be written as $s_{[110]} = m_{[110]}{}^2 \propto \cos^2(\theta_{CF} - \theta_s - \pi/4)$ and $s_{[1\bar{1}0]} = m_{[1\bar{1}0]}{}^2 \propto \sin^2(\theta_{CF} - \theta_s - \pi/4)$, where $s_{[110]}$ and $s_{[1\bar{1}0]}$ represent the area ratio of the [110] and [1$\bar{1}$0] CO patterns, respectively, and $m_{[110]}$ and $m_{[1\bar{1}0]}$ stand for the magnetization

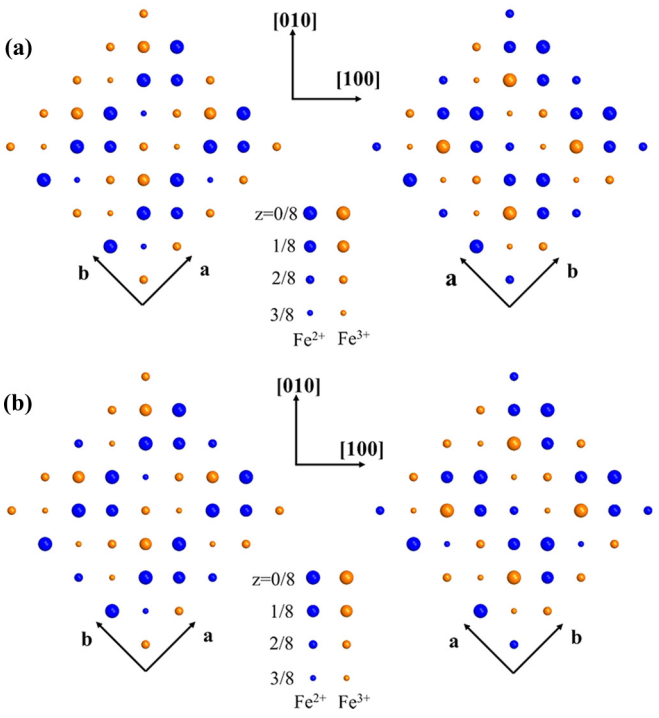

FIG. 6. Schematic drawings of CO patterns of Fe_3O_4 with the separated Fe^{2+} (Fe^{3+}) chains (parallel to the monoclinic a axis) along the [110] (left) and [1$\bar{1}$0] (right) axes in (a) monoclinic $P2/c$ structure and (b) Cc structure, where the blue (brown) balls represent the Fe^{2+} (Fe^{3+}) ions at octahedral sites and the ball size is used to distinguish their positions along the c axis of the crystal with its primitive unit cell length along the c axis being $z = 1$ (top view along the c axis).

component along the [110] and [1$\bar{1}$0] direction during the field cooling process. In this case, the total area should always be 1, and only the [110] (or [1$\bar{1}$0]) CO pattern exists when the CF is along [110] (or [1$\bar{1}$0]). Accordingly, the θ_{CF}-dependent PR angle and ellipticity can be written as

$$\begin{aligned}\delta_c + i\varepsilon_c &= (s_{[110]} - s_{[1\bar{1}0]})(\delta + i\varepsilon) \\ &= (\delta_0 + i\varepsilon_0)\cos 2\theta_s \sin[2(\theta_{CF} - \theta_s)]. \end{aligned} \quad (2)$$

For $\theta_s = 0^\circ$, the expression of the PR angle is reduced to the same equation that we use to fit the twofold symmetry curves in Fig. 4(a). Thus, this provides strong evidence that we can control CO patterns by field cooling in the Fe_3O_4 film with its c axis normal to the plane. So far, the effect of magnetic field cooling on CO has never been reported in the literature; however, it has been shown that magnetite has a slightly lower energy for its magnetization along the a axis than along the b axis [40], thus the separated Fe^{2+} (Fe^{3+}) chains along the a axis have the tendency to align parallel to the CF direction in the field cooling process.

Equation (2) also indicates that the amplitude of the twofold PR angle δ_c should be largest for $\theta_s = 0^\circ$ but become zero for $\theta_s = 45^\circ$. This is because the main optic axis of the birefringence effect induced by the CO is always parallel (or perpendicular) to the polarization of the incident light for $\theta_s = 45^\circ$ so that no PR signal can be expected in this situation. To examine our prediction, we performed the measurements as a function of the azimuthal angle of the sample at $T = 80$ K. Because of the instrument limitations, the sample could be continuously rotated only in a small range ($\sim 15^\circ$), so we needed to reassemble the sample in the dewar system to accomplish the 90° rotation measurement; thus, the absolute value of the PR signal could vary due to the different optic alignment after each sample assembly. However, we could separate the PR signal induced by the CO and the magneto-optical Kerr signal. The Kerr angle is expected to be independent of the sample orientation so that in order to minimize the influence of sample reassembly on the absolute value of the PR signal, we show below the rectified δ_c' the ratio of the absolute δ_c and the magnetic hysteresis loop contrast A_1, i.e., $\delta_c' = \delta_c / A_1$.

Figures 7(a) and 7(b) show the comparison of the rectified PR angle δ_c' obtained at $\theta_s = 0^\circ$ and $\theta_s = 45^\circ$. We noted that δ_c' for $\theta_s = 45^\circ$ also displays a twofold symmetry, but its amplitude is much smaller than that for $\theta_s = 0^\circ$. Moreover, the δ_c' curve for $\theta_s = 45^\circ$ in Fig. 7(b) shows the minima at $\theta_{CF} \sim 45^\circ$ and the maxima at $\theta_{CF} \sim 135^\circ$, which is opposite to that for $\theta_s = 0^\circ$ in Fig. 7(a). Actually, the δ_c' curves for any θ_s all display a twofold symmetry that can be well fitted by a sinusoidal function $\delta_c' = A_2 \cos(2\theta_s)\sin[2\theta_{CF} - \phi_c]$, with the phase ϕ_c depending on θ_s. The amplitude of δ_c' is plotted in Fig. 7(c), showing the maxima at $\theta_s = 0^\circ$ and 90° and a drop to nearly zero when θ_s approaches 45°. This behavior

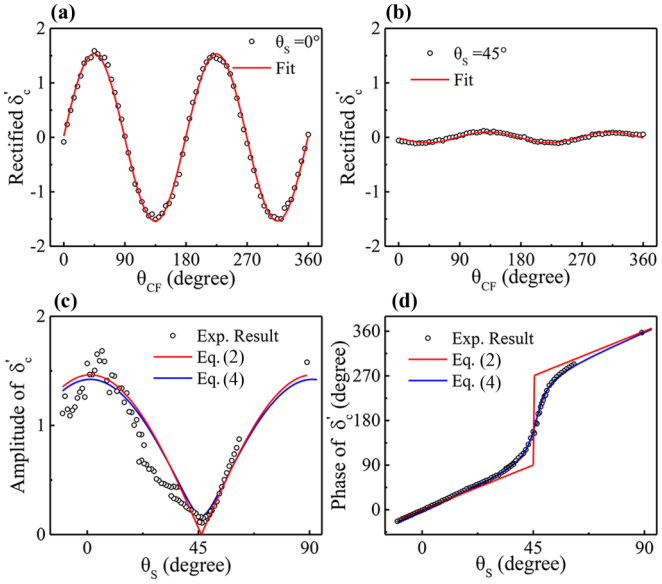

FIG. 7. Rectified twofold δ_c' for (a) $\theta_s = 0°$ and (b) $\theta_s = 45°$ at $T = 80$ K and θ_s dependence of the amplitude (c) and phase (d) of the twofold δ_c'. The solid curves in (a) and (b) are fits by the sinusoidal function. The red curves in (c) and (d) are the fitted curve with Eq. (2). The blue curves in (c) and (d) denote the fits with Eq. (4).

can be reasonably fitted by $|A_2 \cos(2\theta_s)|$ [Fig. 7(c)], in good agreement with the CO-induced birefringence effect.

As can be seen from Eq. (2), the phase ϕ_c of the twofold δ_c should exhibit a linear dependence on θ_s and a jump of 180° when the [110] axis is rotated across the vertical direction ($\theta_s = 45°$). The measured phase ϕ_c indeed displays a linear dependence and 180° phase change in the θ_s range of $0 - 90°$, as shown in Fig. 7(d). However, a significant deviation from the linear dependence occurs near $\theta_s = 45°$. As we have pointed out above, no CO-induced PR signal is expected for the [110] axis parallel to the s polarization, i.e., $\theta_s = 45°$, but we still observed a small PR signal for $\theta_s = 45°$, as shown in Fig. 7(b). Because this twofold PR signal exhibits a 90° phase shift with respect to the CO-induced δ_c, one can understand why ϕ_c displays a significant deviation from linear dependence around $\theta_s = 45°$. This phase shift also indicates the existence of other mechanisms different from the CO pattern to generate the twofold PR signal for $\theta_s = 45°$.

We notice that the monoclinic structure with the c axis within the film plane can result in the PR angle and ellipticity as a function of the CF in the form of

$$\delta_c' = B_2 \sin 2\theta_s \cos[2(\theta_{\rm CF} - \theta_s)]. \quad (3)$$

This PR signal shows a twofold symmetry, and it has a phase shift of 90° with respect to that of the CO-induced twofold δ_c. We thus infer the formation of monoclinic structure with the in-plane c axis within a small fraction of the film, which results in the small remaining twofold δ_c' for $\theta_s = 45°$.

When considering the twofold PR signal induced by both the CO and the in-plane c axis structures, the total PR signal as a function of the CF field orientation $\theta_{\rm CF}$ and sample orientation θ_s can be written as

$$\delta_c' = A_2 \cos(2\theta_s) \sin[2(\theta_{\rm CF} - \theta_s)] + B_2 \sin(2\theta_s) \cos[2(\theta_{\rm CF} - \theta_s)] = A_0 \sin[2\theta_{\rm CF} - \phi_c], \quad (4)$$

where $A_0 = \sqrt{(A_2 \cos 2\theta_s)^2 + (B_2 \sin 2\theta_s)^2}$ and $\phi_c = 2\theta_s + \tan^{-1}(|\frac{B_2}{A_2}| \tan 2\theta_s)$. The phase ϕ_c depends not only on θ_s but also on the ratio of $|B_2/A_2|$. The $\phi_c(\theta_s)$ curve in Fig. 7(d) can be perfectly fitted to Eq. (4). The fitting yields $|B_2/A_2| = 0.119$. The small ratio of $|B_2/A_2|$ indicates that the observed twofold PR signal is dominated by the CO induced by the field cooling. Using this ratio, we recalculated the amplitude of the rectified twofold δ_c' and plotted it as the blue curve in Fig. 7(c).

It should be noted that the above discussions consider only the single atomic structure; however, as shown by the TEM image in Fig. 1(e), the APBs exist in our Fe_3O_4 thin film grown on the MgO substrate because the cation lattice parameter is twice that of the anion lattice [41]. The TEM images reveal that the density of the APBs in our Fe_3O_4 film is similar to that reported in the literature [31,42]. Due to the complicated atomic structure in the APBs, the CO state with two orthogonal orientations can exist only in the antiphase domains surrounded by the APBs. The lattices in the neighboring APB domains may shift 1/4 unit cell along ⟨110⟩ or ⟨100⟩ directions [42] and rotate by 90° for the lattice shift by 1/4 unit cell along the ⟨110⟩ axis. It is important to point out that the CO orientation in different antiphase domains remains along the ⟨110⟩ or ⟨1$\bar{1}$0⟩ axis in spite of these shifts even for a 90° lattice rotation. Field cooling with the CF along the ⟨110⟩ axes may lead to the CO state with single CO orientation parallel to the CF in each antiphase domain, and thus CO states inside all the antiphase domains can be aligned along the same orientation by the field cooling. Therefore, for an ideal sample without any structural defect, it can be expected that the CF could induce the single CO domain with single CO orientation.

B. Ultrafast dynamic behavior of CO

Since the field cooling in our measurement was done with a fs ultrafast laser, we further studied how fast the CO state can be influenced by the ultrafast pump laser. Under the interaction of the pump pulses, we measured δ at $T = 80$ K with $\theta_s = 0°$ and $H = 1000$ Oe using time delayed probe pulses. Figure 8(a) shows δ as a function of θ_H at various time delays Δt. During this PR signal measurement, the pumping pulse was always on, and the field H can be considered as the CF during the field cooling process, i.e., θ_H is equivalent to $\theta_{\rm CF}$. When $\Delta t < 0$, δ shows twofold plus onefold symmetries as the field rotates 360°. In contrast, only the signal with onefold symmetry remains at $\Delta t > 0.8$ ps. This symmetry change is essentially caused by the CO modulated by the pump pulse. The pump pulse instantly heats up the film above T_v at $\Delta t > 0.8$ ps and destroys the CO; thus, δ simply corresponds to the MOKE signal, which changes with the applied field, yielding the PR signal with onefold symmetry. Afterwards, the heat slowly diffuses away, and the sample undergoes field cooling down to 80 K. This cooling process should last longer than 1 ns, since the δ signal only shows the onefold signal up to 1 ns. The cooling process should be finished within 1 ms; thus, a

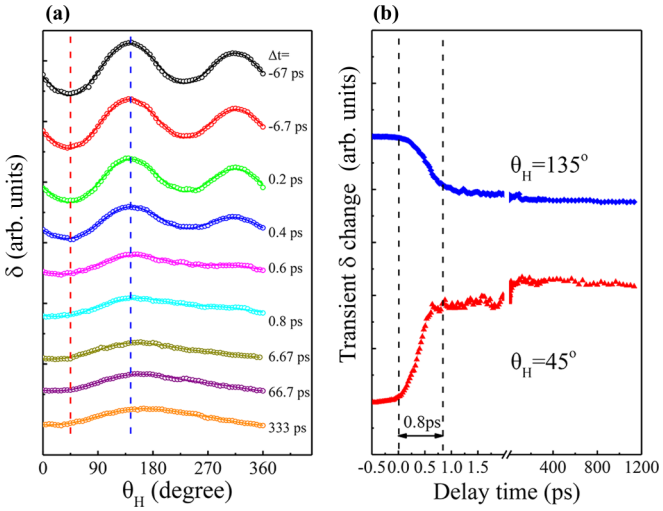

FIG. 8. (a) θ_H-dependent PR angle δ for various time delays after the pump pulse interaction and (b) the time dependent transient δ changes for $\theta_H = 45^\circ$ and 135°.

CO-induced twofold δ_c can be expected to be superimposed on the onefold signal at the negative time delay ($\Delta t \approx 1$ ms). The phase of the twofold δ_c in Fig. 8(a) is opposite to that in the static measurements in Fig. 3, which is caused by the different wavelengths of the probing lights used in the static ($\lambda = 670$ nm) and dynamic ($\lambda = 800$ nm) measurements.

To better resolve the CO dynamics, we modulated the pump laser on and off to measure the transient δ change for a different field angle, θ_H. During this pump-probe measurement, the CF and external field H are essentially identical. Figure 8(b) shows a rapid change of δ immediately after the pump pulse interaction due to the ultrafast melting of the CO state, and a slow recovery longer than 1 ns. The CO melting is complete within ~0.8 ps. This time scale is in agreement with previous experimental results that showed a 1.5 ps time scale for the phase separation to yield residual insulating and metallic regions [43]. Therefore, the PR dynamics further confirm that the observed twofold δ_c originates from the CO state induced by the field cooling.

V. CONCLUSION

In summary, we discovered that the PR of reflected light on a single crystalline Fe_3O_4 film below T_v can be manipulated by ultrafast laser assisted field cooling, which can be well explained by the CF field controlled fractional areas of the two in-plane CO patterns with orthogonal CO orientations below T_v. Our model quantitatively agrees with the PR measurement as a function of sample orientation. The CO state can be melted at an extremely fast rate of less than 0.8 ps by a fs laser pulse. Our findings may help further understand the driving mechanisms of the Verwey transition in magnetite. We propose that the field cooling process is likely to affect CO orientations in other strong correlation systems with magnetoelectric coupling.

ACKNOWLEDGMENTS

The work at the Department of Physics, Fudan University, was supported by the National Key Basic Research Program (Grant No. 2015CB921401), National Key Research and Development Program of China (Grant No. 2016YFA0300703), and the National Natural Science Foundation (Grants No. 11434003, No. 11434074, and No. 11474066) of China. The work at the Department of Optical Science and Engineering, Fudan University, was supported by the National Key Basic Research Program (Grant No. 2015CB921403), National Key Research and Development Program of China (Grant No. 2016YFA0300703), and the National Natural Science Foundation (Grant No. 51371052) of China. We thank Mrs. Münx from Max Planck Institute for Microstructure Physics for her help in preparing TEM samples.

[1] M. Coey, Nature **430**, 155 (2004).
[2] F. Walz, J. Phys.: Condens. Matter, **14**, R285 (2002).
[3] J. García and G. Subías, J. Phys.: Condens. Matter **16**, R145 (2004).
[4] J. P. Attfield, A. M. T. Bell, L. M. Rodriguez-Martinez, J. M. Greneche, R. J. Cernik, J. F. Clarke, and D. A. Perkins, Nature **396**, 655 (1998).
[5] J. C. Loudon, N. D. Mathur, and P. A. Midgley, Nature **420**, 797 (2002).
[6] H. Ichikawa, S. Nozawa, T. Sato, A. Tomita, K. Ichiyanagi, M. Chollet, L. Guerin, N. Dean, A. Cavalleri, S. Adachi, T. Arima, H. Sawa, Y. Ogimoto, M. Nakamura, R. Tamaki, K. Miyano, and S. Koshihara, Nat. Mater. **10**, 101 (2011).
[7] T. Li, A. Patz, L. Mouchliadis, J. Yan, T. A. Lograsso, I. E. Perakis, and J. Wang, Nature **496**, 69 (2013).
[8] C. V. Parker, P. Aynajian, E. H. da. Silva Neto, A. Pushp, S. Ono, J. Wen, Z. Xu, G. Gu, and Y. Ali, Nature **468**, 677 (2010).
[9] T. Wu, H. Mayaffre, S. Krämer, M. Horvatić, C. Berthier, W. N. Hardy, R. Liang, D. A. Bonn, and M. -H. Julien, Nature **477**, 191 (2011).
[10] T. Rohwer, S. Hellmann, M. Wiesenmayer, S. Sohrt, A. Stange, B. Slomski, A. Carr, Y. Liu, L. M. Avila, M. Kalläne, S. Mathias, L. Kipp, K. Rossnagel, and M. Bauer, Nature **471**, 490 (2011).
[11] L. Stojchevska, I. Vaskivskyi, T. Mertelj, P. Kusar, D. Svetin, S. Brazovskii, and D. Mihailovic, Science **344**, 177 (2014).
[12] M. S. Senn, J. P. Wright, and J. P. Attfield, Nature **481**, 173 (2012).
[13] R. Bliem, E. McDermott, P. Ferstl, M. Setvin, O. Gamba, J. Pavelec, M. A. Schneider, M. Schmid, U. Diebold, P. Blaha, L. Hammer, and G. S. Parkinson, Science **346**, 1215 (2014).
[14] C. A. F. Vaz, J. Hoffman, C. H. Ahn, and R. Ramesh, Adv. Mater. **22**, 2900 (2010).
[15] H. Tian, J. Verbeeck, S. Brück, M. Paul, D. Kufer, M. Sing, R. Claessen, and G. Van Tendeloo, Adv. Mater. **26**, 461 (2014).
[16] E. J. W. Verwey, Nature **144**, 327 (1939).
[17] E. J. W. Verwey and P. W. Haayman, Physica **8**, 979 (1941).
[18] J. P. Wright, J. P. Attfield, and P. G. Radaelli, Phys. Rev. B **66**, 214422 (2002).

[19] D. J. Huang, H.-J. Lin, J. Okamoto, K. S. Chao, H.-T. Jeng, G.Y. Guo, C.-H. Hsu, C.-M. Huang, D. C. Ling, W. B. Wu, C. S. Yang, and C. T. Chen, Phys. Rev. Lett. **96**, 096401 (2006).
[20] N. Otsuka and H. Sato, J. Solid State Chem. **61**, 212 (1986).
[21] Z. Kakol, J. Solid State Chem. **88**, 104 (1990).
[22] E. Vittoratos, I. Baranov, and P. P. Meincke, J. Appl. Phys. **42**, 1633 (1971).
[23] K. Moloni, B. M. Moskowitz, and E. D. Dahlberg, Geophys. Res. Lett. **23**, 2851 (1996).
[24] C. H. Li, Phys. Rev. **40**, 1002 (1932).
[25] B. Carter-Stiglitz, B. Moskowitz, P. Solheid, T. S. Berquó, M. Jackson, and A. Kosterov, J. Geophys. Res. **111**, B12S05 (2006).
[26] Z. Ding, B. L. Chen, J. H. Liang, J. Zhu, J. X. Li, and Y. Z. Wu, Phys. Rev. B **90**, 134424 (2014).
[27] C. R. Hu, J. Zhu, G. Chen, J. X. Li, and Y. Z. Wu, Phys. Lett. A **376**, 3317 (2012).
[28] X. H. Liu, A. D. Rata, C. F. Chang, A. C. Komarek, and L. H. Tjeng, Phys. Rev. B **90**, 125142 (2014).
[29] R. Ramos, S. K. Arora, and I. V. Shvets, Phys. Rev. B **78**, 214402 (2008).
[30] P. J. van der Zaag, W. F. J. Fontijn, P. Gaspard, R. M. Wolf, V. A. M. Brabers, R. J. M. van de Veerdonk, and P. A. A. van der Heijden, J. Appl. Phys. **79**, 5936 (1996).
[31] W. Eerenstein, T. T. M. Palstra, T. Hibma, and S. Celotto, Phys. Rev. B **68**, 014428 (2003).
[32] Z. Q. Qiu and S. D. Bader, Rev. Sci. Instrum. **71**, 1243 (2000).
[33] T. P. Ma, S. F. Zhang, Y. Yang, Z. H. Chen, H. B. Zhao, and Y. Z. Wu, J. Appl. Phys. **117**, 013903 (2015).
[34] To minimize the effect of the laser drift on the δ_c, we fixed $H_E = 1000$ Oe along the [100] axis and measured the PR for $\theta_{\mathrm{CF}} = 0^\circ$ each time before measuring PR for other θ_{CF}. The δ_c shown in Fig. 4(a) is obtained by subtraction of such two PR signals.
[35] M. S. Senn, J. P. Wright, J. Cumby, and J. P. Attfield, Phys. Rev. B **92**, 024104 (2015).
[36] I. Leonov, A. N. Yaresko, V. N. Antonov, M. A. Korotin, and V. I. Anisimov, Phys. Rev. Lett. **93**, 146404 (2004).
[37] K. Yamauchi, T. Fukushima, and S. Picozzi, Phys. Rev. B **79**, 212404 (2009).
[38] R. Takahashi, H. Misumi, and M. Lippmaa, Phys. Rev. B **86**, 144105 (2012).
[39] A. D. Rowan, C. H. Patterson, and L. V. Gasparov, Phys. Rev. B **79**, 205103 (2009).
[40] H. J. Williams, R. M. Bozorth, and M. Goertz, Phys. Rev. **91**, 1107 (1953).
[41] D. T. Margulies, F. T. Parker, F. E. Spada, R. S. Goldman, J. Li, R. Sinclair, and A. E. Berkowitz, Phys. Rev. B **53**, 9175 (1996).
[42] T. Hibma, F. C. Voogt, L. Niesen, P. A. A. van der Heijden, W. J. M. de Jonge, J. J. T. M. Donkers, and P. J. van der Zaag, J. Appl. Phys. **85**, 5291 (1999).
[43] S. de Jong, R. Kukreja, C. Trabant, N. Pontius, C. F. Chang, T. Kachel, M. Beye, F. Sorgenfrei, C. H. Back, B. Bräuer, W. F. Schlotter, J. J. Turner, O. Krupin, M. Doehler, D. Zhu, M. A. Hossain, A. O. Scherz, D. Fausti, F. Novelli, M. Esposito *et al.*, Nat. Mater. **12**, 882 (2013).